Water Science & Technology

IWA PUBLISHING

Water Science & Technology Vol 84 No 5, 1190 doi: 10.2166/wst.2021.312

Response surface design for removal of Cr(VI) by hydrogel-supported sulfidated nano zero-valent iron (S-nZVI@H)

Qi Jing*, Wenhui You, Le Tong, Wenyu Xiao, Siyan Kang and Zhongyu Ren

Faculty of Architecture, Civil and Transportation Engineering, Beijing University of Technology, Beijing 100124, China
*Corresponding author. E-mail: jingqi@bjut.edu.cn

QJ, 0000-0002-2965-3828

ABSTRACT

In this study, a new sulfidated nanoscale zero-valent iron (S-nZVI) supported on hydrogel (S-nZVI@H) was successfully synthesized for the removal of chromium (Cr) (VI) from groundwater. The surface morphology, dispersion phenomenon and functional groups of novel S-nZVI@H were characterized by scanning electron microscopy and Fourier transform infrared spectroscopy. Box–Behnken design (BBD) optimization technology based on response surface methodology (RSM) is applied to demonstrate the influence of the interaction of S-nZVI@H dose, initial Cr(VI) concentration, contact time, and initial pH with the Cr(VI) removal efficiency. The analysis of variance results ($F = 118.73$, $P < 0.0001$, $R^2 = 0.9916$) show that the quadratic polynomial model is significant enough to reflect the close relationship between the experimental and predicted values. The predicted optimum removal conditions are: S-nZVI@H dose 9.46 g/L, initial Cr(VI) concentration 30 mg/L, contact time 40.7 min, and initial pH 5.27, and the S-nZVI@H dose is the key factor affecting the removal of Cr(VI). The predicted value (99.76%) of Cr (VI) removal efficiency is in good agreement with the experimental value (97.75%), which verifies the validity of the quadratic polynomial model. This demonstrates that RSM with appropriate BBD can be utilized to optimize the design of experiments for removal of Cr(VI).

Key words: Box–Behnken design, Cr(VI), hydrogel, optimization, S-nZVI, sulfidation

HIGHLIGHTS

- Hydrogel-supported sulfidated zero-valent iron nanoparticle (S-nZVI@H) was successfully prepared and used to remove Cr(VI) from groundwater.
- The effect of the interaction of four independent variables on the removal efficiency of Cr(VI) was studied by RSM.
- The optimum removal conditions and key factors for Cr(VI) removal were determined.
- BBD is considered to optimize the experimental study of Cr(VI) removal by S-nZVI@H.

INTRODUCTION

As a metal pollutant, chromium (Cr) comes from industrial processes such as tanning, electroplating, metallurgy, and textile (Selvi *et al.* 2001). Large quantities of Cr-containing wastewater are drained into rivers, resulting in contamination of soil and groundwater. Cr usually exists in the environment in the form of trivalent chromium (Cr(III)) and hexavalent chromium (Cr(VI)) (Fendorf 1995). The toxicity of Cr(VI) is higher than that of Cr(III) mainly because of its higher solubility, fluidity, and bioavailability (Kotaś & Stasicka 2000). Cr(VI) can increase the risk of cancer by entering the body through direct contact with the skin or inhalation (Gheju 2011; Zhu *et al.* 2017). In order to effectively control the pollution of Cr, some methods of removing Cr(VI) have been developed, including activated carbon adsorption technology (Mohan & Pittman Jr 2006), polymer membrane filtration technology (Aroua *et al.* 2007), ion exchange technology (Lin & Kiang 2003), electrochemical precipitation technology (Kongsricharoern & Polprasert 1995). In order to further improve the removal efficiency of Cr(VI) and reduce the impact of the treatment processes on the environment, it is necessary to develop a green material with high removal efficiency, low cost, and little secondary pollution.

In recent years, nanomaterials have been widely applied in the removal of pollutants from water (Eskandari *et al.* 2018; Galdames *et al.* 2020; Li *et al.* 2021; Tsade *et al.* 2021). Among them, nano zero-valent iron (nZVI) has been widely used in the remediation of groundwater and soil pollution due to its high specific surface area and reactivity (Zhang 2003).

Nevertheless, nZVI particles have a number of limitations that affect their reaction with contaminants. (1) nZVI easily aggregates based on the action of van der Waals force and magnetic force, and eventually reduces the migration in aquifer (Phenrat *et al.* 2007; Israelachvili *et al.* 2008; Li *et al.* 2017b). (2) nZVI particles with extremely high reactivity can react with other substances in the water in addition to the target contaminants, resulting in poor selectivity for pollutants (Cai *et al.* 2020; He *et al.* 2020). (3) When using nZVI in practice, a passivation layer can easily form on the surface of nZVI prohibiting the Fe^0 core to react with pollutants, thus lowering the reactivity (Sarathy *et al.* 2008). The bare nZVI therefore needs to be modified to improve these limitations. A common approach is to load the nZVI onto inorganic carriers such as bentonite (Chen *et al.* 2011b) and biochar (Su *et al.* 2016). The author applied diatomite to support nZVI to remove Cr(VI) from water and achieved better dispersion and lower oxidation degree of nZVI with high removal rate (Zhang *et al.* 2019). In addition, the coating of polymer on the surface of nZVI is also an effective method. Chen *et al.* (2011a) conducted an experimental study on the removal of tetracycline from polluted water by modified nZVI with polyvinylpyrrolidone (PVP-K30). Another method for the modification of nZVI is adding transition metal to nZVI to form a bimetallic iron base. Zhu *et al.* (2016) reported the method of adding Cu metal to nZVI to repair Cr(VI) in groundwater.

The higher reactivity, selectivity, and lifetime of nZVI based on sulfidation are considered as promising characteristics (Xie & Cwiertny 2010; Fan *et al.* 2016a, 2017; Xu *et al.* 2020b). At present, there are two commonly used methods for the preparation of sulfide nanoparticles. Kim *et al.* (2011) used a facile one-pot synthesis process by adding a mixture of dithionite and sodium borohydride ($NaBH_4$) to a solution of ferric iron (Fe^{3+}) to synthesize Fe/FeS nanoparticles, achieving high reduction rate for trichloroethylene (TCE). Another method of sulfidation is to reduce ferrous iron (Fe^{2+}) with $NaBH_4$ and then add Na_2S, commonly known as the two-step synthesis method (Rajajayavel & Ghoshal 2015). Sulfurization breaks the application limit of nZVI. Fan *et al.* (2016a) reported that sulfidation of nZVI enhances the rate of dechlorination of TCE, indicating that the corrosion reaction with water of nZVI is suppressed. In view of improving lifetime of S-nZVI, Xie & Cwiertny (2010) proposed that the reduction ability of aged nZVI could be restored by using dithionite as a reducing agent to sulfurize the nZVI to prolong its lifetime. In addition, sulfidation significantly increases the crystal domain size and lattice spacing of iron. The larger lattice constant is beneficial for the electron transfer, thus improving the reactivity and selectivity for the reduction of contaminants (Xu *et al.* 2020a). These achievements are impressive and indicate that S-nZVI has great potential for the removal of pollutants from water (Su *et al.* 2015; Li *et al.* 2016, 2017a, 2020).

In order to improve the aggregation phenomenon and anti oxidation property of S-nZVI, using a porous material as the supported carrier of nanoparticles is an effective choice. Chen *et al.* (2020) removed TCE from groundwater by loading S-nZVI on biochar (BC). The promotion of removal and degradation of TCE benefited from the high adsorption capacity of BC and the high reduction capacity of S-nZVI. Other researchers have also applied inorganic porous material to support S-nZVI for the removal of heavy metal (Su *et al.* 2015; Qu *et al.* 2021) and toxic dye (Yang *et al.* 2018). Based on its strong response to environmental stimulation, biocompatibility, swelling property, and elasticity, hydrogels have been used in drug transportation, eyeglasses manufacturing, biosensor development, artificial muscles, and other aspects (Manetti *et al.* 2002; Sahiner *et al.* 2006; Satarkar & Zach Hilt 2008; Fuhrer *et al.* 2009; Jain *et al.* 2017). In this study, organic hydrogels with non-toxic, environmentally friendly, cheap and porous properties were selected as the carrier of S-nZVI. Hydrogel has super function of absorbing contaminants (Jin *et al.* 2009; Sahiner & Ilgin 2010) due to the three-dimensional (3D) network formed by cross-linking of polymer chains. In addition, hydrogels also have hydrophilic functional groups such as COOH, OH, $CONH_2$, and NH_2 in the structure, where negatively charged COOH can be combined with positively charged metal ions (Cu^{2+} and Fe^{2+}) in aqueous solution by electrostatic forces (Chauhan *et al.* 2006; Sahiner *et al.* 2010a). Consequently, hydrogels can be used as reaction containers for in-situ reduction of metal nanoparticles (Sahiner 2006; Sahiner *et al.* 2010b). The metal nanoparticles are uniformly dispersed in the hydrogel network system, thus avoiding the serious aggregation of nanoparticles. Furthermore, hydrogels can be used as a protective structure to reduce the oxidation degree of nanoparticles to a certain extent. Obviously, it is worth expecting to combine S-nZVI with hydrogel (S-nZVI@H) to form a novel material to fully amplify the super reduction ability of S-nZVI particles, and then repair the pollution of Cr(VI) in groundwater.

Response surface methodology (RSM) is a design method that combines mathematics and statistics to establish polynomial models based on experimental data (Bezerra *et al.* 2008). After determining independent variables, designing experiments, data statistics, and model validation, the goal of determining the optimal independent variable conditions is achieved. Box–Behnken design (BBD) is one of the optimization analysis methods in the quadratic response surface design method,

which can show the influence of interaction between multiple variables on the response value and avoid the combination of all variables in extreme circumstances (Ferreira *et al.* 2007; Bezerra *et al.* 2008).

In this study, nZVI@H and S-nZVI@H were synthesized and characterized for the removal of Cr(VI). Scanning electron microscopy (SEM) and Fourier transform infrared spectroscopy (FTIR) were applied to survey the surface morphology, dispersion phenomenon, and structure of original hydrogels, nZVI, nZVI@H, and S-nZVI@H. Comparison experiments were performed to research the removal efficiency of nZVI@H and S-nZVI@H. Considering the removal efficiency, S-nZVI@H was selected as the material for the response surface experiment design. The S-nZVI@H dose, initial Cr(VI) concentration, contact time, and initial pH were taken as independent variables to explore the influence of the interaction of four independent variables on the Cr(VI) removal efficiency to acquire the optimal conditions for removal Cr(VI).

MATERIALS AND METHODS

Materials

Analytical pure levels of chemicals and reagents were used in this study. Ferrous sulfate ($FeSO_4{\cdot}7H_2O$), sodium hydrosulfite ($Na_2S_2O_4$), and sodium borohydride ($NaBH_4$) were purchased from Tianjin Fuchen Chemical Reagent Factory (Tianjin, China). The solution required in the experiment was mixed with deionized water. Hydrochloric acid (HCl, 0.1 mol/L) and sodium hydroxide (NaOH, 0.1 mol/L) were used to adjust the pH of the solution.

Preparation of S-nZVI@H

The prepared sodium polyacrylate and polyacrylamide were copolymerized in a constant temperature water bath and dried to obtain the PANa-PAM hydrogel used in this study. The S-nZVI was prepared by one-pot method initiated by Kim *et al.* (2011). The S-nZVI@H composites were prepared by supporting S-nZVI on hydrogel. First, hydrogel globules were dipped in ferrous sulfate solution (0.1 mol/L) for 24 h. After soaking, the hydrogel globules were filtered with deionized water three times to remove Fe^{2+} on its surface. Then, a three-necked flask was prepared to fill the soaked hydrogel globules, which were immersed in deionized water. S-nZVI@H were prepared by liquid phase reduction method. For the preparation of the reaction solution, $NaBH_4$ (1 mol/L) and $Na_2S_2O_4$ (0.1 mol/L) were put into the 250 mL conical flask and dissolved by stirring with 200 mL of deionized water. The reductant solution was injected into the three-neck flask at 28 L/min through a peristaltic pump in nitrogen atmosphere and stirred at 90 rpm for 1 h. The reaction process of zero-valent iron (Fe^0) is exhibited in Equation (1):

$$FeSO_4 + 2NaBH_4 + 6H_2O \rightarrow Fe^0 + 2B(OH)_3 + Na_2SO_4 + 7H_2\uparrow \quad (1)$$

The formation of FeS occurs during the reduction of Fe^{2+}, which is shown in Equations (2)–(5):

$$2S_2O_4^{2-} + H_2O \rightarrow 2HSO_3^- + S_2O_3^{2-} \quad (2)$$

$$S_2O_4^{2-} + S_2O_3^{2-} + 2H_2O + H^+ \rightarrow H_2S + 3HSO_3^- \quad (3)$$

$$H_2S \rightarrow 2H^+ + S^{2-} \quad (4)$$

$$Fe^{2+} + S^{2-} \rightarrow FeS \quad (5)$$

The acquired S-nZVI@H composites were immersed in deionized water for 2 h in the presence of nitrogen to remove the residual $NaBH_4$ and $Na_2S_2O_4$. Finally, the fresh S-nZVI@H were dried in a freeze drier (FD-1 A-50) for 24 h.

Characterization of the hydrogel, nZVI, nZVI@H, and S-nZVI@H

The surface morphology and microscopic structure of the hydrogel, nZVI, nZVI@H, and S-nZVI@H were observed with SEM (JSM-7610F-Plus, JEOL Ltd, Japan). The functional groups of the hydrogel, nZVI, nZVI@H, and S-nZVI@H were analyzed using a FTIR (IRAffinity-1S, Shimadzu, Japan).

Cr(VI) removal batch experiments

Removal experiments were deployed using 250 mL conical flask containing 200 mL Cr(VI) solution at 25 °C. Different masses of potassium dichromate were taken and dissolved in deionized water with different pH values. Afterwards, various

dosages of S-nZVI@H were added inside a conical flask with a certain concentration of Cr(VI) solution, which were shaken evenly at 180 rpm at a constant temperature (DSHZ-33A) of 25 °C. Solution was withdrawn by injection syringe at certain reaction time intervals. The concentration of the reaction solution was determined at 540 nm by a UV–visible spectrophometer (2082SUV/VIS) using diphenylcarboxyl dihydrazine spectrophotometry method. Finally, the efficiency of Cr(VI) removal was calculated using Equation (6):

$$\text{Cr(VI) removal efficiency}(\%) = \frac{C_0 - C}{C_0} \times 100\% \tag{6}$$

where C_0 is the initial concentrations (mol/L) of Cr(VI) and C is the concentrations (mol/L) after removal at a certain time.

Experimental design

In the content of this study, BBD was applied to conduct the RSM to acquire the optimal conditions for removal and the most significant factor affecting the removal. Practical optimization steps and the main content of this work are as follows: (1) determination of independent variables with relatively significant influence; (2) batch experiments of removal at determined conditions; (3) establishing the mathematical model by quadratic polynomial function fitting with experimental data; (4) calculating the optimal conditions for removal and the independent variable of most significant effect; and (5) conducting a validation experiment under the given optimal removal conditions obtained from the previous fitting procedure. The S-nZVI@H dose (A), the initial Cr(VI) concentration (B), contact time (C), and initial pH (D) are selected as independent variables. The Cr(VI) removal efficiency is set to the predicted response value. The influence of the interaction of four independent variables and one response value is described by using the quadratic polynomial model (Equation (7)).

$$R = b_0 + b_1\mathrm{A} + b_2\mathrm{B} + b_3\mathrm{C} + b_4\mathrm{D} + b_{12}\mathrm{AB} + b_{13}\mathrm{AC} + b_{14}\mathrm{AD} + b_{23}\mathrm{BC} + b_{24}\mathrm{BD} + b_{34}\mathrm{CD} + b_{11}\mathrm{A}^2 + b_{22}\mathrm{B}^2 + b_{33}\mathrm{C}^2 + b_{44}\mathrm{D}^2 \tag{7}$$

where R is the predicted response value of Cr(VI) removal, b_0 is the intercept value; $b_1 - b_4$ are the linear coefficients; $b_{12} - b_{14}$, $b_{23} - b_{24}$ and b_{34} are the cross-product coefficients; $b_{11} - b_{44}$ are the quadratic coefficients; A, B, C, and D are the code forms of the input variables (Gopinath *et al.* 2010).

In this study, the experimental data are coded and analyzed with Design-Expert 8.0.6 Trial. Four independent variables and their levels are listed in Table 1. The experimental design procedure and results of Cr(VI) removal are shown in Table 2. Twenty-nine groups of experiments are designed, which includes five parallel experiments. Analysis of variance (ANOVA) is used to determine the fitting degree between the values obtained from the experiment and the predicted response values calculated by the regression mode (Silveira *et al.* 2017). The statistical significance is evaluated by the coefficient of determination R^2 (Khosravi & Arabi 2016).

RESULTS AND DISCUSSION

Characterizations of the hydrogel, nZVI, nZVI@H, and S-nZVI@H

FTIR was used to reveal the chemical functional groups of PANa-PAM hydrogel, nZVI, nZVI@H, and S-nZVI@H (Figure 1). The broad peak around 3,420 cm^{-1} is assigned to hydroxyl groups (Dong *et al.* 2018). The peak near 2,370 cm^{-1} is the saturated zone of CO_2 (Dong *et al.* 2018). The peak at 1,310 cm^{-1} is attributed to C–C stretching (Tang *et al.* 2008). The

Table 1 | Experimental domain and levels of independent variables

			Level		
Variables	**Unit**	**Factors**	**Low (−1)**	**Middle (0)**	**High (+1)**
S-nZVI@H dose	g/L	A	2	6	10
Initial Cr(VI) concentration	mg/L	B	10	20	30
Contact time	min	C	5	25	45
Initial pH	/	D	4	6	8

Table 2 | The coding values of the four independent variables and the experimental and predicted values of Cr(VI) removal

Run	A (g/L)	B (mg/L)	C (min)	D (/)	Experimental (%)	Predicted (%)
1	0	0	1	−1	86.07	84.07
2	0	1	0	−1	78.39	79.33
3	0	0	0	0	79.99	82.07
4	0	−1	0	1	82.93	81.77
5	0	1	1	0	84.31	81.91
6	0	−1	0	−1	82.93	84.03
7	0	−1	1	0	91.94	90.88
8	−1	1	0	0	20.88	22.13
9	0	0	0	0	82.93	82.07
10	0	0	0	0	79.52	82.07
11	1	0	0	−1	87.93	84.01
12	1	0	−1	0	44.71	44.04
13	1	1	0	0	84.93	87.02
14	−1	0	0	−1	40.02	41.78
15	0	0	−1	1	25.08	28.92
16	−1	−1	0	0	51.16	50.91
17	1	−1	0	0	84.34	84.93
18	−1	0	0	1	21.37	23.66
19	−1	0	−1	0	8.19	2.68
20	0	0	−1	−1	45.64	47.76
21	0	0	0	0	83.96	82.07
22	0	1	0	1	61.10	59.78
23	1	0	0	1	83.73	80.34
24	0	0	0	0	83.96	82.07
25	−1	0	1	0	38.40	38.85
26	0	0	1	1	81.39	81.12
27	0	−1	−1	0	50.22	51.00
28	0	1	−1	0	33.84	33.28
29	1	0	1	0	91.10	96.39

absorption peaks at 1,670 cm^{-1}, 1,570 cm^{-1}, and 1,390 cm^{-1} are assigned to C = O stretching, the N–H bending and –C–N– deformation of the $–CONH_2$ group in the hydrogel, respectively (Tang *et al.* 2008; Dong *et al.* 2019). Likewise, the absorption peak at around 1,420 cm^{-1} is attributed to the symmetric stretching vibration of the $–COO^-$ anions in the hydrogel (Tang *et al.* 2008). These absorption peaks of the hydrogel also present in nZVI@H and S-nZVI@H, indicating that nZVI and S-nZVI have been successfully supported by hydrogels. The adsorption peak at about 470 cm^{-1} corresponds to Fe–O stretches due to the oxidation of nZVI in the air (Zhang *et al.* 2011). Occurrence of less obvious Fe–O stretches in nZVI@H and S-nZVI@H may be caused by the fact that the degree of oxidation of these two materials is modestly inhibited. The new band spectrum at 1,100 cm^{-1} and 830 cm^{-1} of S-nZVI@H compared with the infrared images of nZVI@H further indicates that nZVI has been successfully sulfidation (Chernyshova 2003; Reyes-Bozo *et al.* 2015).

SEM was applied to elucidate the surface morphology and structure of PANa-PAM hydrogel, nZVI, nZVI@H, and S-nZVI@H. The porous network structure of PANa-PAM hydrogel is clearly observed in Figure 2(a). The spherical structure of bare nZVI is shown in Figure 2(b). It can be observed that the diameter of nZVI particles is less than 100 nm with aggregation. The surface morphologies of nZVI@H and S-nZVI@H are shown in Figure 2(c) and 2(d), respectively. The porous structure of the supported hydrogel retains a rougher surface. Both nZVI and S-nZVI particles are successfully loaded in

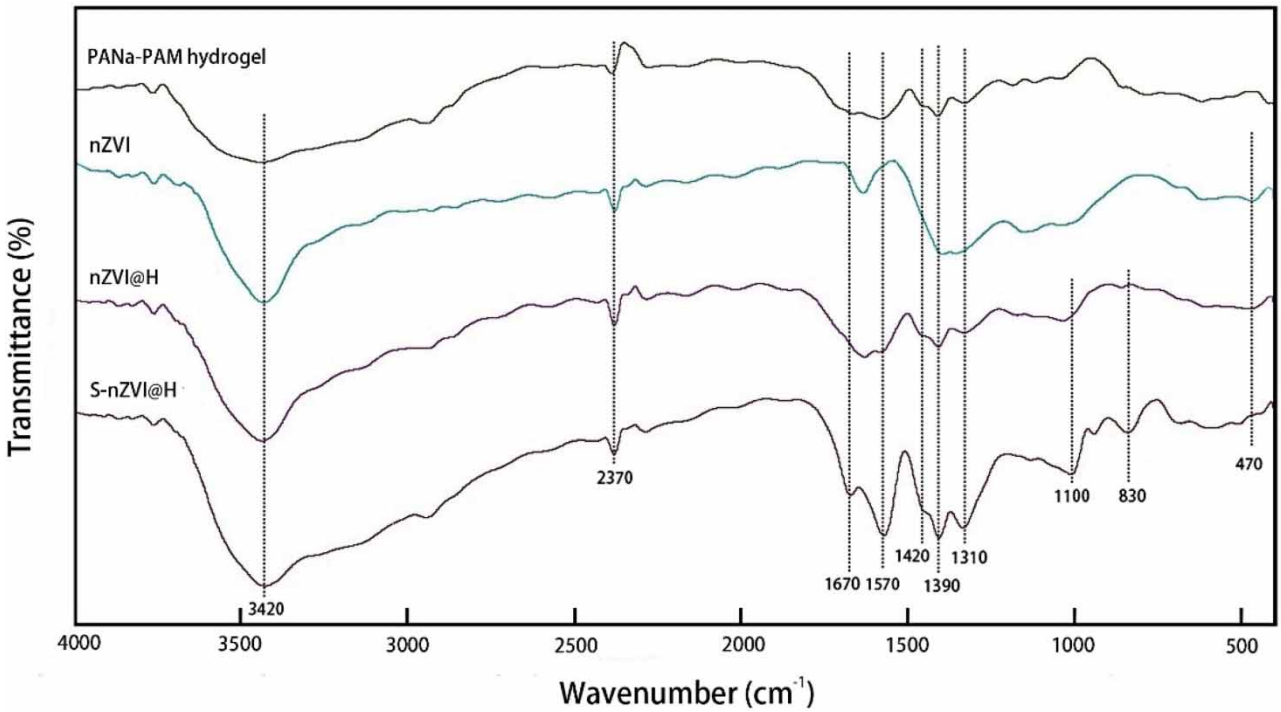

Figure 1 | FTIR analysis of the hydrogel, nZVI, nZVI@H, and S-nZVI@H.

the hydrogel as small bulges in granular form and their dispersion performance is relatively better than that of bare nZVI. The unique 3D structure of PANa-PAM hydrogel can effectively inhibit the aggregation of nanoparticles. It is obvious from Figure 2(d) that the size of S-nZVI particles distributed in the porous hydrogel is larger and has a uniform distribution, which may be due to the minimization of aggregation by electrostatic repulsion and steric hindrance in the case of sulfidation.

Comparison of removal of Cr(VI) between nZVI@H and S-nZVI@H

According to previous studies on S-nZVI, the reactivity and selectivity of S-nZVI with pollutants are greatly enhanced compared with bare nZVI (Fan *et al.* 2016b, 2017). A comparative experiment was conducted to further explore Cr(VI) removal efficiency of S-nZVI@H and nZVI@H under certain experimental conditions (initial Cr(VI) concentration of 20 mg/L, pH 6, nZVI@H and S-nZVI@H dosage of 6 g/L, and temperature of 25 °C). Figure 3 shows that the removal efficiency of nZVI@H and S-nZVI@H increases rapidly in the first 30 min. After 60 min, the Cr(VI) removal efficiencies of both reach more than 90%. The removal efficiency of S-nZVI@H is 24.89% higher than that of nZVI@H at 5 min. During the reaction of Cr(VI) and S-nZVI@H, the sulfur species FeS enhances the transfer of electrons from the core to the surface of nZVI, thus increasing the probability of Cr(VI) reduction (Li *et al.* 2018; Brumovský *et al.* 2021). Brumovský *et al.* (2021) verified that S-nZVI was more effective in removing Cr(VI) than nZVI in laboratory conditions. Additionally, Su *et al.* (2015) reported that S-nZVI had a higher surface area rather than bare nZVI, generating more metal ion adsorption binding sites. Accordingly, the reason why S-nZVI@H can remove Cr(VI) more quickly and effectively compared with nZVI@H is that sulfidation can improve the dispersity of nZVI and selectivity of nZVI to Cr(VI). Specifically, sulfidation of nZVI reduces the magnetic interaction between nZVI nanoparticles by the formation of an iron sulfide compound, as a result of ameliorating the aggregation. Moreover, the outer layer created by sulfidation decreases the direct reaction of nZVI with water, thus improving the electron selectivity for the reduction of Cr(VI) and extending its reactive lifetime. PANa-PAM hydrogel, in particular, provides a protective layer for the passivation of S-nZVI, and makes S-nZVI more evenly distributed in the hydrogel network, thus improving the reduction effectivity of Cr(VI). Therefore, the removal of Cr(VI) by S-nZVI@H was further analyzed by RSM.

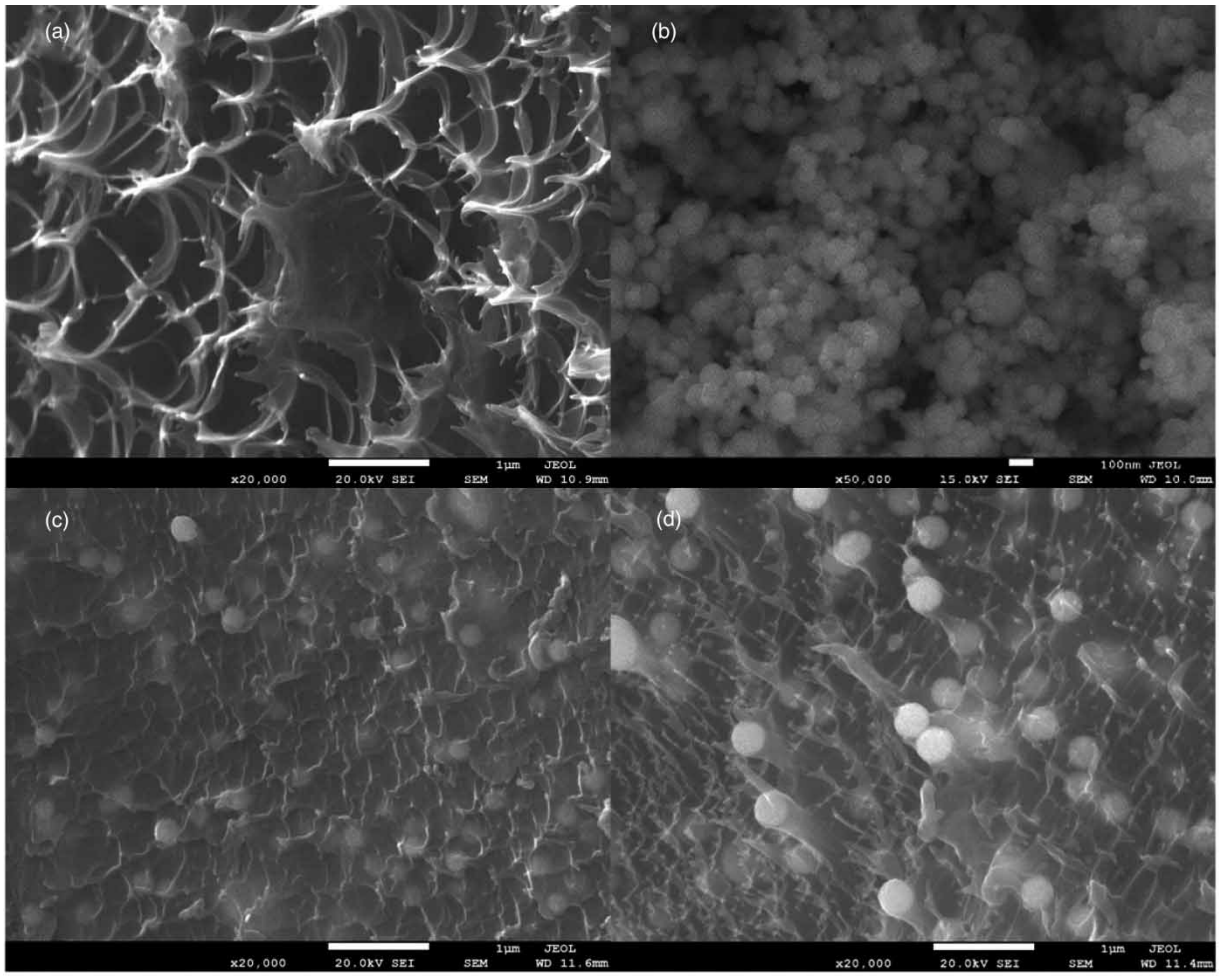

Figure 2 | SEM images of (a) hydrogel, (b) nZVI, (c) nZVI@H, (d) S-nZVI@H.

Model fitting results and analysis

BBD experiment design was carried out through 29 batch experiments. The quadratic polynomial equation of the relationship between the four independent variables and the predicted response value of Cr(VI) removal is obtained in Equation (8):

$$R = 82.07 + 24.73A - 6.67B + 22.13C - 5.45D + 7.72AB + 4.04AC + 3.61AD + 2.19BC - 4.32BD + 3.97CD - 19.80A^2 - 1.02B^2 - 16.78C^2 - 4.82D^2 \quad (8)$$

The predicted response value of Cr(VI) removal is calculated according to Equation (8), and the calculated results are presented in Table 2. To understand the fitting effect between the predicted response values and the experimental values in detail, the fitting curve between them was obtained by RSM. Figure 4 shows that data points are distributed at both ends of the straight line and most of them are distributed on the straight line. The coefficient of determination (R^2) of the linear equation is 0.9916, which indicates the quadratic polynomial model has better fitting degree and higher accuracy. The root mean squares error (RMSE = 2.32) and the absolute average deviation (AAD = 5.39) of the model were calculated according to Equations (9) and (10). RMSE and AAD are parameters that evaluate the difference (Liu *et al.* 2009) and the degree of regression (Zheng *et al.* 2020) between the predicted response values of the model and the experimental values, respectively.

$$\mathrm{RMSE} = \left[\frac{1}{n}\sum_{i=1}^{n}(y_i - y_b)^2\right]^{\frac{1}{2}} \quad (9)$$

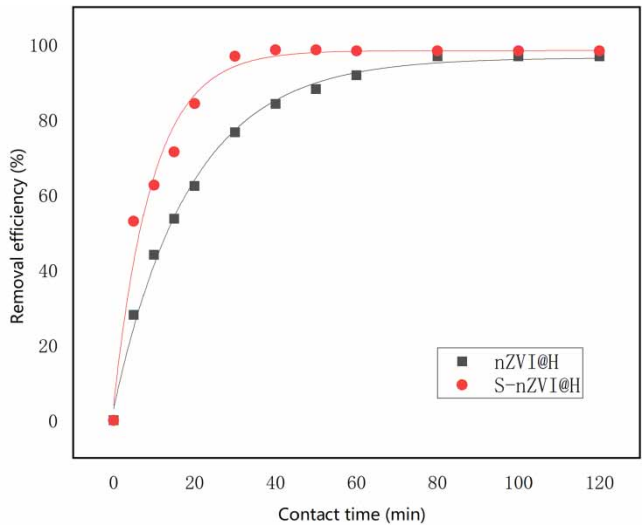

Figure 3 | Removal efficiencies of Cr(VI) by nZVI@H and S-nZVI@H.

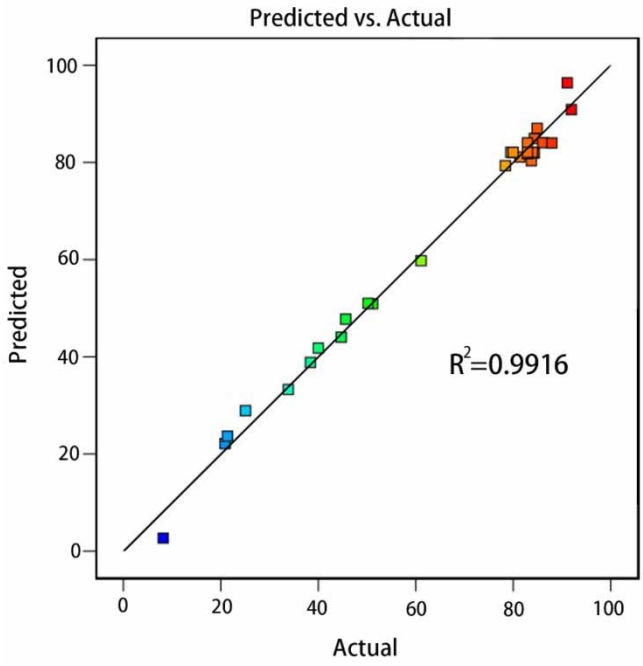

Figure 4 | Scatter plot of actual and predicted values of Cr(VI) removal by S-nZVI@H.

$$\mathrm{AAD} = \frac{\sum_{i}^{n}\left(\frac{|y_b - y_a|}{y_a}\right)}{n} \times 100 \tag{10}$$

where n is the number of experiments, y_b is the predicted response value, and y_a is the experimental value (Sohrabi *et al.* 2014).

ANOVA is used to evaluate the regression significance of quadratic polynomial model and the non-significance of inadequate fitting. The fitting degree of the model is evaluated by F-value, P-value, lack-of-fit, and R^2 to verify the quality and reliability of the model (Mohammadi *et al.* 2017). With the larger F-value and the smaller P-value, the significance of the model is higher. The model is logical when the F-value of the model is greater than the critical F-value. The critical F-value is calculated according to $F_{0.05,\,df,\,(n-df+1)}$. $F_{0.05,14,14}$ is 2.484 according to the F test threshold table. The critical

F-value is less than the calculated F-value. As can be seen from Table 3, the F-value of the model is equal to 118.73 and *P*-value is less than 0.05, which indicates that the model is significantly effective (Mansouriieh *et al.* 2019). Among the four model items A, B, C, and D, item A has the largest F-value, indicating that the dosage of S-nZVI@H has a significant effect on the predicted response value of the model, which can be used as the key factor for Cr(VI) removal. Furthermore, the F-value of D is smaller than that of the other three items, indicating that the initial pH value of solution has little influence on the predicted response value of the model. The F-value of lack-of-fit is equal to 2.92, which is not obvious, indicating that it is not important in model fitting compared with pure error. Meanwhile, due to noise, there is 15.64% probability of the F-value missing. The degree of dispersion of data points is reflected by the square root of the variance (Std.dev (3.33)) and the ratio of standard deviation to mean value (coefficient of variation (CV) (5.17)). A smaller value of CV indicates that the data points and mean value are approaching, which means that the reliability of the model is higher. The predicted residual sum of squares (PRESS) is used to measure the responsive ability of the model to predict the experiment, and the model is ideal when the value of PRESS is small (Sohrabi *et al.* 2014). Adeq precision represents the signal to noise ratio (SNR). According to Table 3, the SNR is equal to 39.096 and the value is greater than 4, indicating that this model is reliable to predict experiments (Beg *et al.* 2003; Sohrabi *et al.* 2014). R^2 (Equation (11)) is the ratio of the sum of squares of the model (SS_{Model}) to the sum of squares of the total (SS_{Total}), which can be used to evaluate the degree of fitting between experimental values and predicted values of the model (Mansouriieh *et al.* 2019). The R^2 should be within the range from zero to one ($0 \leq R^2 \leq 1$). The closer R^2 is to 1, the better the model fitting effect is.

$$R^2 = \frac{SS_{Model}}{SS_{Total}} \tag{11}$$

Table 3 | The ANOVA results for the response surface model for the removal of Cr(VI)

Source	Sum of squares	df	Mean square	F-value	*P*-value	
Model	18,461.55	14	1,318.68	118.73	<0.0001	Significant
A	7,336.90	1	7,336.90	660.58	<0.0001	
B	534.27	1	534.27	48.10	<0.0001	
C	5,875.52	1	5,875.52	529.00	<0.0001	
D	356.21	1	356.21	32.07	<0.0001	
AB	238.24	1	238.24	21.45	0.0004	
AC	65.45	1	65.45	5.89	0.0293	
AD	52.20	1	52.20	4.70	0.0479	
BC	19.14	1	19.14	1.72	0.2104	
BD	74.74	1	74.74	6.73	0.0212	
CD	63.04	1	63.04	5.68	0.0319	
A^2	2,542.79	1	2,542.79	228.94	<0.0001	
B^2	6.79	1	6.79	0.61	0.4473	
C^2	1,827.06	1	1,827.06	164.50	<0.0001	
D^2	150.50	1	150.81	13.58	0.0024	
Residual	155.50	14	11.11			
Lack-of-fit	136.78	10	13.68	2.92	0.1564	Not significant
Pure error	18.71	4	4.68			
Cor total	1,8617.05	28				
Std. dev	3.33		R-squared	0.9916		
Mean	64.52		Adj R-squared	0.9833		
CV	5.17		Pred R-square	0.9561		
PRESS	817.11		Adeq precision	39.0964		

The calculated R^2 is 0.9916 (Table 3), which indicates that there is a 99.16% probability that the predicted value of the model has a linear relationship with the experimental value. Adjusted R-squared (0.9833) and predicted R-squared (0.9561) of the regression line are presented in Table 3. Obviously, these two values are close to each other and can well express the predicted response value of the model under the condition of adjusted R-squared.

The residual graph is drawn to verify whether the residual of the model has the characteristics of normality, independence, and constancy (Un *et al.* 2014). Figure 5(a) is the residual normal possibility diagram, which indicates that the distribution of residuals conforms to the characteristics of Gaussian distribution, thus verifying the normal distribution characteristics of residuals. The chronological diagram of residuals is shown in Figure 5(b). Residual values are distributed between −3.93 and 3.93 with irregular distribution characteristics, which shows the independence of residuals. If the model is correct and reliable, the residual does not exhibit a special structure and does not have a relationship with other variables (Mansouriieh *et al.* 2019). Figure 5(c) is the residual graph based on predicted values. The distribution of residuals within a certain range is also irregular, which shows the constancy of residuals. The smaller residual is when the residual data points are close to the zero line. The more residual data points close to the zero line, the better the fitting degree between the predicted value and the experimental value. These three residual diagrams show that the quadratic polynomial model established by RSM has certain reliability and can effectively predict the experimental results.

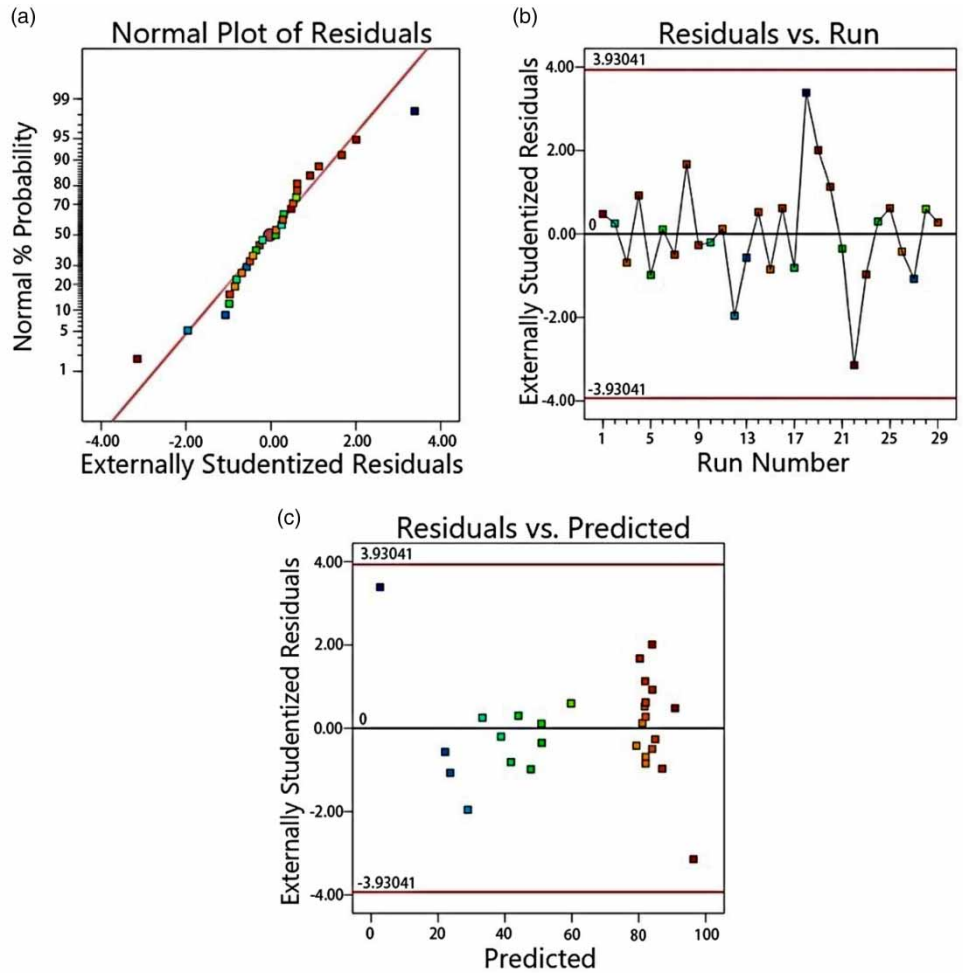

Figure 5 | Residual plots of Cr(VI) removal efficiency using S-nZVI@H, (a) residuals normal possibility diagram, (b) the chronological diagram of residuals, (c) residuals graph based on predicted values.

3D response surface analysis

Based on the quadratic polynomial model, the 3D response surface map can visualize the relationship between the interaction of the two independent variables and the Cr(VI) removal efficiency while keeping the other two variables fixed. Figure 6 shows the effects of the interaction between two of the four independent variables (S-nZVI@H dose (A), initial Cr(VI) concentration (B), contact time (C), and initial pH (D)) on the removal efficiency of Cr(VI) by S-nZVI@H. In each response surface diagram, under certain two variables, the highest point of the surface is the best reaction condition under which the maximum removal efficiency can be obtained.

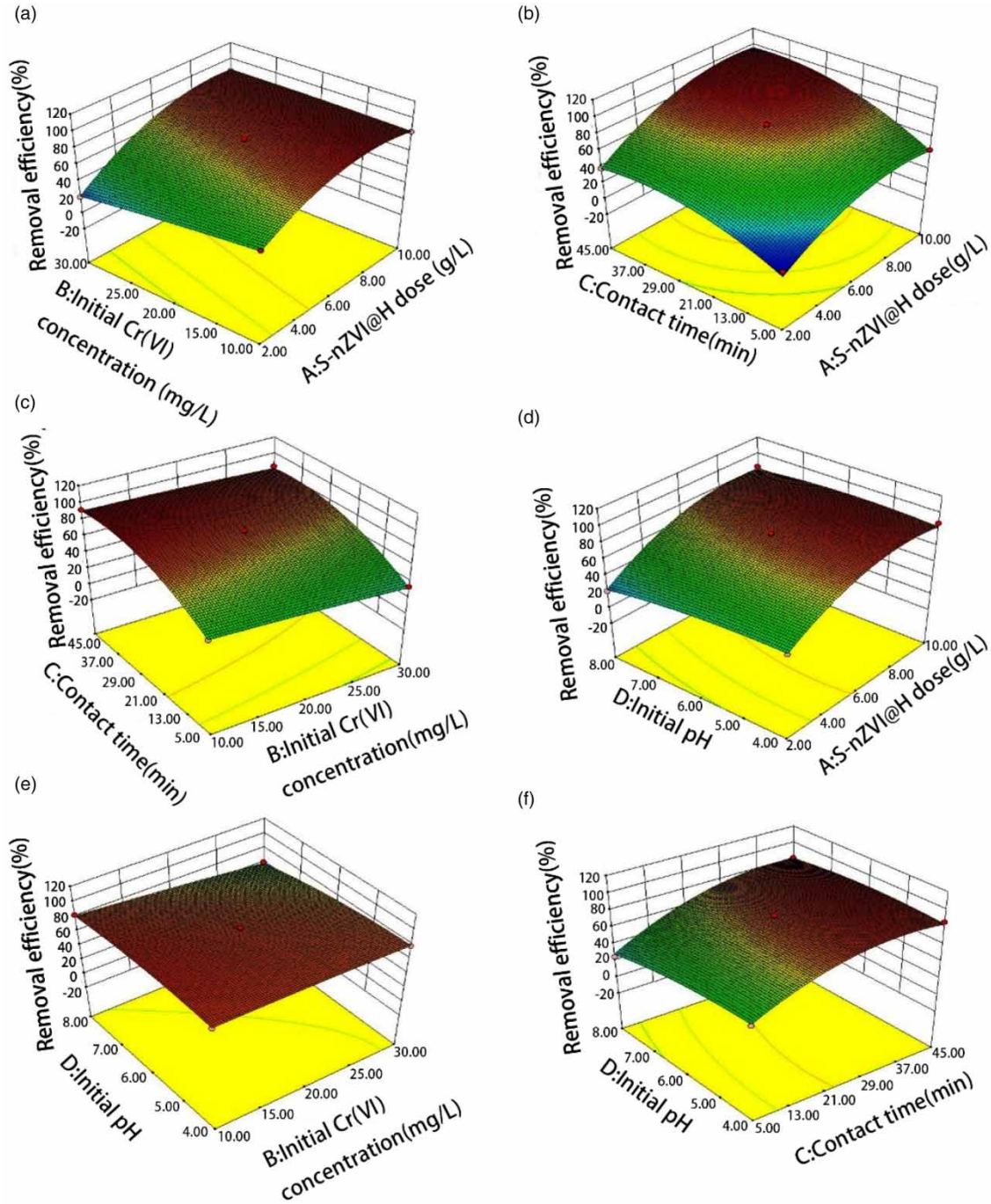

Figure 6 | 3D diagrams showing interactive influence of (a) S-nZVI@H dose and initial Cr(VI) concentration, (b) S-nZVI@H dose and contact time, (c) initial Cr(VI) concentration and contact time, (d) S-nZVI@H dose and initial pH, (e) initial Cr(VI) concentration and initial pH, (f) contact time and initial pH on Cr(VI) removal by S-nZVI@H.

The interactive impact of the combination of S-nZVI@H dose and initial Cr(VI) concentration on Cr(VI) removal efficiency is presented in Figure 6(a). It shows that the removal efficiency increases with decreasing initial Cr(VI) concentration and increasing S-nZVI@H dose. S-nZVI@H can provide more surface-active sites, improving the reduction ability of Cr(VI). The higher the initial concentration of Cr (VI), the more surface-active sites of S-nZVI can be occupied, resulting in the lower removal efficiency of Cr(VI) (Khosravi & Arabi 2016). At S-nZVI@H dose 7.72 g/L and initial Cr(VI) concentration 10.10 mg/L, a maximum Cr(VI) removal of 91.36% is determined.

The reciprocal effect of contact time and S-nZVI@H dose on Cr(VI) removal efficiency is shown in Figure 6(b). As S-nZVI@H dose and contact time increases, the removal efficiency of Cr(VI) improves. The removal efficiency of Cr(VI) increases rapidly at the initial contact time, which indicates that the reduction of Cr(VI) is predominant (Ponder *et al.* 2000). However, with the further extension of contact time, the Cr(VI) removal efficiency increases slowly, which is due to the accumulation of Fe(III)–Cr(III) hydroxides on the surface of S-nZVI@H hindering the reaction between Cr(VI) and S-nZVI (Wu *et al.* 2015; Li *et al.* 2017c). In addition, it can be clearly observed that the curvature of the surface is relatively large, which indicates that the interaction of contact time and S-nZVI@H dose has a great influence on the Cr(VI) removal efficiency. A maximum Cr(VI) removal (98.95%) is observed at S-nZVI@H dose of 8.76 g/L and contact time of 39.57 min.

Figure 6(c) shows the combined effect of initial Cr(VI) concentration and contact time on removal of Cr(VI). With the increase of contact time and the decrease of initial Cr(VI) concentration, the removal efficiency of Cr(VI) increases continuously. The extended contact time provides sufficient reaction time for the reduction and adsorption of Cr(VI) by S-nZVI@H. Under the condition of higher initial Cr(VI) concentration, the removal efficiency of Cr(VI) is reduced. This can be attributed to the limited number of active sites provided by a fixed amount of S-nZVI@H. At initial Cr(VI) concentration 10.02 mg/L and contact time 36.39 min, a maximum Cr(VI) removal of 93.63% is determined.

The plot for interactive effect of S-nZVI@H dose and initial pH (Figure 6(d)) shows that increasing initial pH results in a decreasing removal of Cr(VI); conversely, this increases with the increase of S-nZVI@H dose. This is because, under alkaline conditions, nZVI appears electronegative; under acidic conditions, nZVI appears electropositive (Gong *et al.* 2017). Cr(VI) exists mainly in the form of $HCrO_4^-$ in acidic conditions, and only in the form of CrO_4^{2-} in alkaline solutions (Lv *et al.* 2011). Obviously, in alkaline solution, negatively charged nZVI and CrO_4^{2-} are more likely to generate electrostatic repulsion, which inhibits their interaction, leading to the decrease of Cr(VI) removal. A maximum Cr(VI) removal (90.33%) is determined at S-nZVI@H dose 8.30 g/L and initial pH 5.3.

The interactive influence of initial Cr(VI) concentration and initial pH on Cr(VI) removal is shown in Figure 6(e). Under the dual function of high pH value and high initial Cr(VI) concentration, the removal efficiency of Cr(VI) is reduced. Moreover, it can be observed that the curvature of the response surface is small, which indicates that the interaction between initial Cr(VI) concentration and initial pH has a slight influence on the removal efficiency of Cr(VI). At initial Cr(VI) concentration 10.07 mg/L and initial pH 3.72, a maximum Cr(VI) removal of 87.72% is determined.

The interaction of contact time and initial pH on Cr(VI) removal is shown in Figure 6(f). It may be noted that the trend of Cr(VI) removal efficiency is consistent with the change of contact time and is contrary to the initial pH. Similarly, the contact time and the initial pH play the same role as stated above. A maximum Cr(VI) removal (89.8%) is determined at contact time of 37.61 min and initial pH of 5.38.

Model validation

As an optimization technology, RSM needs to be verified for its adaptability (Bezerra *et al.* 2008). To evaluate the validity and feasibility of the RSM model, three parallel experiments were carried out under the conditions of independent variables corresponding to the maximum Cr(VI) removal efficiency determined by the model (Table 4). The predicted optimum removal

Table 4 | Results of three parallel experiments under the predicted optimum removal conditions

Optimum conditions					Verification test		
S-nZVI@H dose (g/L)	Initial Cr(VI) concentration (mg/L)	Contact time (min)	Initial pH	Predicted removal efficiency (%)	Experimental removal efficiency (%)	Mean value (%)	Relative error of prediction (%)
9.46	30	40.7	5.27	99.76	97.62 98.11 97.53	97.75	2.07

conditions obtained from RSM are S-nZVI@H dose (9.46 g/L), initial Cr(VI) concentration (30 mg/L), contact time (40.7 min), and initial pH (5.27). The relative error of prediction between the mean value of the experimental (97.75%) and predicted (99.76%) removal efficiency was calculated as 2.07%, which showed that the quadratic polynomial model can well predict the removal of Cr(VI) by S-nZVI@H (Ashrafi *et al.* 2018).

CONCLUSIONS

In this study, two materials of nZVI@H and S-nZVI@H are successfully synthesized for Cr(VI) removal. With better removal effects confirmed by SEM and FTIR characterizations and comparable experiments, S-nZVI@H is selected as the material designed by RSM to further explore its removal efficiency of Cr(VI). Furthermore, BBD experimental design is used to reveal the influence of the interaction of four independent variables on the Cr(VI) removal efficiency and the predicted optimum removal conditions are: S-nZVI@H dose 9.46 g/L, initial Cr(VI) concentration 30 mg/L, contact time 40.7 min, and initial pH 5.27. Additionally, the S-nZVI@H dose is the key factor affecting the removal of Cr(VI). The variance analysis and residual analysis of the experimental data are carried out by quadratic polynomial model. The analysis results show that the correlation between the experimental values and the predicted values is high ($F = 118.73$, $P < 0.0001$, $R^2 = 0.9916$), which corroborates the quality and reliability of the model. To verify the validity and feasibility of the model, three parallel experiments are carried out under the predicted optimum removal conditions. The removal efficiency of S-nZVI@H for Cr(VI) obtained from the experiment (97.75%) is very close to the predicted value of the model (99.76%). In conclusion, BBD based on RSM can be used to statistically optimize the experimental study of Cr(VI) removal by S-nZVI@H.

ACKNOWLEDGEMENT

The authors thank the National Natural Science Foundation of China (No. 41907176) for supporting this project.

DATA AVAILABILITY STATEMENT

All relevant data are included in the paper or its Supplementary Information.

REFERENCES

Aroua, M. K., Zuki, F. M. & Sulaiman, N. M. 2007 Removal of chromium ions from aqueous solutions by polymer-enhanced ultrafiltration. *Journal of Hazardous Materials* **147** (3), 752–758. doi:10.1016/j.jhazmat.2007.01.120.

Ashrafi, M., Bagherian, G., Arab Chamjangali, M. & Goudarzi, N. 2018 Removal of brilliant green and crystal violet from mono- and Bi-component aqueous solutions using NaOH-modified walnut shell. *Analytical and Bioanalytical Chemistry Research* **5** (1), 95–114. doi:10.22036/abcr.2018.106139.1172.

Beg, Q. K., Sahai, V. & Gupta, R. 2003 Statistical media optimization and alkaline protease production from *Bacillus mojavensis* in a bioreactor. *Process Biochemistry* **39** (2), 203–209. doi:10.1016/S0032-9592(03)00064-5.

Bezerra, M. A., Santelli, R. E., Oliveira, E. P., Villar, L. S. & Escaleira, L. A. 2008 Response surface methodology (RSM) as a tool for optimization in analytical chemistry. *Talanta* **76** (5), 965–977. doi:10.1016/j.talanta.2008.05.019.

Brumovský, M., Oborná, J., Lacina, P., Hegedüs, M., Sracek, O., Kolařík, J., Petr, M., Kašlík, J., Hofmann, T. & Filip, J. 2021 Sulfidated nanoscale zerovalent iron is able to effectively reduce in situ hexavalent chromium in a contaminated aquifer. *Journal of Hazardous Materials* **405**, 124665. doi:10.1016/j.jhazmat.2020.124665.

Cai, S., Chen, B., Qiu, X., Li, J., Tratnyek, P. G. & He, F. 2020 Sulfidation of zero-valent iron by direct reaction with elemental sulfur in water: efficiencies, mechanism, and dechlorination of trichloroethylene. *Environmental Science & Technology*. doi:10.1021/acs.est.0c05397.

Chauhan, G. S., Singh, B., Sharma, R. K., Verma, M., Chauhan Jaswal, S. & Sharma, R. 2006 Use of biopolymers and acrylamide-based hydrogels for sorption of Cu^{2+}, Fe^{2+} and Cr^{6+} ions from their aqueous solutions. *Desalination* **197** (1–3), 75–81. doi:10.1016/j.desal.2005.12.017.

Chen, H., Luo, H., Lan, Y., Dong, T., Hu, B. & Wang, Y. 2011a Removal of tetracycline from aqueous solutions using polyvinylpyrrolidone (PVP-K30) modified nanoscale zero-valent iron. *Journal of Hazardous Materials.* doi:10.1016/j.jhazmat.2011.04.089.

Chen, Z., Jin, X., Chen, Z., Megharaj, M. & Naidu, R. 2011b Removal of methyl orange from aqueous solution using bentonite-supported nanoscale zero-valent iron. *Journal of Colloid and Interface Science* **363** (2), 601–607. doi:10.1016/j.jcis.2011.07.057.

Chen, J., Dong, H., Tian, R., Li, R. & Xie, Q. 2020 Remediation of trichloroethylene-contaminated groundwater by sulfide-modified nanoscale zero-valent iron supported on biochar: investigation of critical factors. *Water, Air, & Soil Pollution* **231** (8). doi:10.1007/s11270-020-04797-3.

Chernyshova, I. V. 2003 An in situ FTIR study of galena and pyrite oxidation in aqueous solution. *Journal of Electroanalytical Chemistry* **558**, 83–98. doi:10.1016/S0022-0728(03)00382-6.

Dong, H., Zhang, C., Deng, J., Jiang, Z., Zhang, L., Cheng, Y., Hou, K., Tang, L. & Zeng, G. 2018 Factors influencing degradation of trichloroethylene by sulfide-modified nanoscale zero-valent iron in aqueous solution. *Water Research* **135**, 1–10. doi:10.1016/j.watres.2018.02.017.

Dong, H., Cheng, Y., Lu, Y., Hou, K., Zhang, L., Li, L., Wang, B., Wang, Y., Ning, Q. & Zeng, G. 2019 Comparison of toxicity of Fe/Ni and starch-stabilized Fe/Ni nanoparticles toward *Escherichia coli*. *Separation and Purification Technology* **210**, 504–510. https://doi.org/10.1016/j.seppur.2018.08.042.

Eskandari, M., Goudarzi, N. & Moussavi, S. G. 2018 Application of low-voltage UVC light and synthetic ZnO nanoparticles to photocatalytic degradation of ciprofloxacin in aqueous sample solutions. *Water and Environment Journal* **32** (1), 58–66. https://doi.org/10.1111/wej.12291.

Fan, D., O'Brien Johnson, G., Tratnyek, P. G. & Johnson, R. L. 2016a Sulfidation of nano zerovalent iron (nZVI) for improved selectivity during in-situ chemical reduction (ISCR). *Environmental Science & Technology* **50** (17), 9558–9565. doi:10.1021/acs.est.6b02170.

Fan, D., O'Carroll, D. M., Elliott, D. W., Xiong, Z., Tratnyek, P. G., Johnson, R. L. & Garcia, A. N. 2016b Selectivity of nano zerovalent iron in in situ chemical reduction: challenges and improvements. *Remediation Journal* **26** (4), 27–40. doi:10.1002/rem.21481.

Fan, D., Lan, Y., Tratnyek, P. G., Johnson, R. L., Filip, J., O'Carroll, D. M., Nunez Garcia, A. & Agrawal, A. 2017 Sulfidation of iron-based materials: a review of processes and implications for water treatment and remediation. *Environmental Science & Technology* **51** (22), 13070–13085. doi:10.1021/acs.est.7b04177.

Fendorf, S. E. 1995 Surface reactions of chromium in soils and waters. *Geoderma* **67** (1), 55–71. doi:10.1016/0016-7061(94)00062-F.

Ferreira, S. L. C., Bruns, R. E., Ferreira, H. S., Matos, G. D., David, J. M., Brandão, G. C., Da Silva, E. G. P., Portugal, L. A., Dos Reis, P. S., Souza, A. S. & Dos Santos, W. N. L. 2007 Box–Behnken design: an alternative for the optimization of analytical methods. *Analytica Chimica Acta* **597** (2), 179–186. doi:10.1016/j.aca.2007.07.011.

Fuhrer, R., Athanassiou, E. K., Luechinger, N. A. & Stark, W. J. 2009 Crosslinking metal nanoparticles into the polymer backbone of hydrogels enables preparation of soft, magnetic field-driven actuators with muscle-like flexibility. *Small* **5** (3), 383–388. doi:10.1002/smll.200801091.

Galdames, A., Ruiz-Rubio, L., Orueta, M., Sánchez-Arzalluz, M. & Vilas-Vilela, J. L. 2020 Zero-valent iron nanoparticles for soil and groundwater remediation. *International Journal of Environmental Research and Public Health* **17** (16), 5817. doi:10.3390/ijerph17165817.

Gheju, M. 2011 Hexavalent chromium reduction with zero-valent iron (ZVI) in aquatic systems. *Water, air, and Soil Pollution* **222** (1), 103–148. doi:10.1007/s11270-011-0812-y.

Gong, Y., Gai, L., Tang, J., Fu, J., Wang, Q. & Zeng, E. Y. 2017 Reduction of Cr(VI) in simulated groundwater by FeS-coated iron magnetic nanoparticles. *Science of The Total Environment* **595**, 743–751. doi:10.1016/j.scitotenv.2017.03.282.

Gopinath, K. P., Muthukumar, K. & Velan, M. 2010 Sonochemical degradation of Congo Red: optimization through response surface methodology. *Chemical Engineering Journal* **157** (2–3), 427–433. doi:10.1016/j.cej.2009.12.002.

He, F., Gong, L., Fan, D., Tratnyek, P. G. & Lowry, G. V. 2020 Quantifying the efficiency and selectivity of organohalide dechlorination by zerovalent iron. *Environmental Science: Processes & Impacts* **22** (3), 528–542. doi:10.1039/C9EM00592G.

Israelachvili, J., Min, Y., Kristiansen, K., Golan, Y. & Akbulut, M. 2008 The role of interparticle and external forces in nanoparticle assembly. *Nature Materials* **7** (7), 527–538. doi:10.1038/nmat2206.

Jain, D., Karajic, A., Murawska, M., Goudeau, B., Bichon, S., Gounel, S., Mano, N., Kuhn, A. & Barthélémy, P. 2017 Low-molecular-weight hydrogels as new supramolecular materials for bioelectrochemical interfaces. *ACS Applied Materials & Interfaces* **9** (1), 1093–1098. doi:10.1021/acsami.6b12890.

Jin, L., Lu, P., You, H., Chen, Q. & Dong, J. 2009 Vitamin B12 diffusion and binding in crosslinked poly(acrylic acid)s and poly(acrylic acid-co-N-vinyl pyrrolidinone)s. *International Journal of Pharmaceutics* **371** (1–2), 82–88. doi:10.1016/j.ijpharm.2008.12.022.

Khosravi, M. & Arabi, S. 2016 Application of response surface methodology (RSM) for the removal of methylene blue dye from water by nano zero-valent iron (NZVI). *Water Science and Technology* **74** (2), 343–352. doi:10.2166/wst.2016.122.

Kim, E., Kim, J., Azad, A. & Chang, Y. 2011 Facile synthesis and characterization of Fe/FeS nanoparticles for environmental applications. *ACS Applied Materials & Interfaces* **3** (5), 1457–1462. doi:10.1021/am200016v.

Kongsricharoern, N. & Polprasert, C. 1995 Electrochemical precipitation of chromium (Cr^{6+}) from an electroplating wastewater. *Water Science and Technology* **31** (9), 109–117. doi:10.2166/wst.1995.0350.

Kotaś, J. & Stasicka, Z. 2000 Chromium occurrence in the environment and methods of its speciation. *Environmental Pollution (1987)* **107** (3), 263–283. doi:10.1016/S0269-7491(99)00168-2.

Li, D., Mao, Z., Zhong, Y., Huang, W., Wu, Y. & Peng, P. A. 2016 Reductive transformation of tetrabromobisphenol A by sulfidated nano zerovalent iron. *Water Research* **103**, 1–9. doi:10.1016/j.watres.2016.07.003.

Li, D., Zhu, X., Zhong, Y., Huang, W. & Peng, P. 2017a Abiotic transformation of hexabromocyclododecane by sulfidated nanoscale zerovalent iron: kinetics, mechanism and influencing factors. *Water Research* **121**, 140–149. doi:10.1016/j.watres.2017.05.019.

Li, J., Zhang, X., Sun, Y., Liang, L., Pan, B., Zhang, W. & Guan, X. 2017b Advances in sulfidation of zerovalent iron for water decontamination. *Environmental Science & Technology* **51** (23), 13533–13544. doi:10.1021/acs.est.7b02695.

Li, Y., Wang, W., Zhou, L., Liu, Y., Mirza, Z. A. & Lin, X. 2017c Remediation of hexavalent chromium spiked soil by using synthesized iron sulfide particles. *Chemosphere (Oxford)* **169**, 131–138. doi:10.1016/j.chemosphere.2016.11.060.

Li, J., Zhang, X., Liu, M., Pan, B., Zhang, W., Shi, Z. & Guan, X. 2018 Enhanced reactivity and electron selectivity of sulfidated zerovalent iron toward chromate under aerobic conditions. *Environmental Science & Technology* **52** (5), 2988–2997. doi:10.1021/acs.est.7b06502.

Li, P., Lin, K., Fang, Z. & Zhang, W. 2020 Degradation of nitrate and secondary pollution in drinking water by S-NZVI prepared from steel pickling waste liquor. *Journal of Hydro-Environment Research* **28**, 15–21.

Li, H., Huang, Y., Liu, J. & Duan, H. 2021 Hydrothermally synthesized titanate nanomaterials for the removal of heavy metals and radionuclides from water: a review. *Chemosphere* **282**, 131046. https://doi.org/10.1016/j.chemosphere.2021.131046.

Lin, S. H. & Kiang, C. D. 2003 Chromic acid recovery from waste acid solution by an ion exchange process: equilibrium and column ion exchange modeling. *Chemical Engineering Journal (Lausanne, Switzerland: 1996)* **92** (1), 193–199. doi:10.1016/S1385-8947(02)00140-7.

Liu, Y., Hu, N., Wang, H. & Li, P. 2009 Soft chemical analyzer development using adaptive least-squares support vector regression with selective pruning and variable moving window size. *Industrial & Engineering Chemistry Research* **48** (12), 5731–5741. doi:10.1021/ie8012709.

Lv, X., Xu, J., Jiang, G. & Xu, X. 2011 Removal of chromium(VI) from wastewater by nanoscale zero-valent iron particles supported on multiwalled carbon nanotubes. *Chemosphere* **85** (7), 1204–1209. doi:10.1016/j.chemosphere.2011.09.005.

Manetti, C., Casciani, L. & Pescosolido, N. 2002 Diffusive contribution to permeation of hydrogel contact lenses: theoretical model and experimental evaluation by nuclear magnetic resonance techniques. *Polymer* **43** (1), 87–92. doi:10.1016/S0032-3861(01)00559-6.

Mansouriieh, N., Sohrabi, M. R. & Khosravi, M. 2019 Optimization of profenofos organophosphorus pesticide degradation by zero-valent bimetallic nanoparticles using response surface methodology. *Arabian Journal of Chemistry* **12** (8), 2524–2532. doi:10.1016/j.arabjc.2015.04.009.

Mohammadi, A., Nemati, S., Mosaferi, M., Abdollahnejhad, A., Almasian, M. & Sheikhmohammadi, A. 2017 Predicting the capability of carboxymethyl cellulose-stabilized iron nanoparticles for the remediation of arsenite from water using the response surface methodology (RSM) model: modeling and optimization. *Journal of Contaminant Hydrology* **203**, 85–92. doi:10.1016/j.jconhyd.2017.06.005.

Mohan, D. & Pittman Jr, C. U. 2006 Activated carbons and low cost adsorbents for remediation of tri- and hexavalent chromium from water. *Journal of Hazardous Materials* **137** (2), 762–811. doi:10.1016/j.jhazmat.2006.06.060.

Phenrat, T., Saleh, N., Sirk, K., Tilton, R. D. & Lowry, G. V. 2007 Aggregation and sedimentation of aqueous nanoscale zerovalent iron dispersions. *Environmental Science & Technology* **41** (1), 284–290. doi:10.1021/es061349a.

Ponder, S. M., Darab, J. G. & Mallouk, T. E. 2000 Remediation of Cr(VI) and Pb(II) aqueous solutions using supported, nanoscale zero-valent iron. *Environmental Science & Technology* **34** (12), 2564–2569. doi:10.1021/es9911420.

Qu, J., Liu, Y., Cheng, L., Jiang, Z., Zhang, G., Deng, F., Wang, L., Han, W. & Zhang, Y. 2021 Green synthesis of hydrophilic activated carbon supported sulfide nZVI for enhanced Pb(II) scavenging from water: characterization, kinetics, isotherms and mechanisms. *Journal of Hazardous Materials* **403**, 123607. doi:10.1016/j.jhazmat.2020.123607.

Rajajayavel, S. R. C. & Ghoshal, S. 2015 Enhanced reductive dechlorination of trichloroethylene by sulfidated nanoscale zerovalent iron. *Water Research* **78**, 144–153. doi:10.1016/j.watres.2015.04.009.

Reyes-Bozo, L., Escudey, M., Vyhmeister, E., Higueras, P., Godoy-Faúndez, A., Salazar, J. L., Valdés-González, H., Wolf-Sepúlveda, G. & Herrera-Urbina, R. 2015 Adsorption of biosolids and their main components on chalcopyrite, molybdenite and pyrite: zeta potential and FTIR spectroscopy studies. *Minerals Engineering* **78**, 128–135. doi:10.1016/j.mineng.2015.04.021.

Sahiner, N. 2006 In situ metal particle preparation in cross-linked poly(2-acrylamido-2-methyl-1-propansulfonic acid) hydrogel networks. *Colloid and Polymer Science* **285** (3), 283–292. doi:10.1007/s00396-006-1562-z.

Sahiner, N. & Ilgin, P. 2010 Multiresponsive polymeric particles with tunable morphology and properties based on acrylonitrile (AN) and 4-vinylpyridine (4-VP). *Polymer* **51** (14), 3156–3163. doi:10.1016/j.polymer.2010.04.060.

Sahiner, N., Godbey, W. T., McPherson, G. L. & John, V. T. 2006 Microgel, nanogel and hydrogel–hydrogel semi-IPN composites for biomedical applications: synthesis and characterization. *Colloid and Polymer Science* **284** (10), 1121–1129. doi:10.1007/s00396-006-1489-4.

Sarathy, V., Tratnyek, P. G., Nurmi, J. T., Baer, D. R., Amonette, J. E., Chun, C. L., Penn, R. L. & Reardon, E. J. 2008 Aging of iron nanoparticles in aqueous solution: effects on structure and reactivity. *The Journal of Physical Chemistry C* **112** (7), 2286–2293. doi:10.1021/jp0777418.

Sahiner, N., Ozay, H., Ozay, O. & Aktas, N. 2010a A soft hydrogel reactor for cobalt nanoparticle preparation and use in the reduction of nitrophenols. *Applied Catalysis B: Environmental* **101** (1–2), 137–143. doi:10.1016/j.apcatb.2010.09.022.

Sahiner, N., Ozay, H., Ozay, O. & Aktas, N. 2010b New catalytic route: hydrogels as templates and reactors for in situ Ni nanoparticle synthesis and usage in the reduction of 2- and 4-nitrophenols. *Applied Catalysis A: General* **385** (1–2), 201–207. doi:10.1016/j.apcata.2010.07.004.

Satarkar, N. S. & Zach Hilt, J. 2008 Hydrogel nanocomposites as remote-controlled biomaterials. *Acta Biomaterialia* **4** (1), 11–16. doi:10.1016/j.actbio.2007.07.009.

Selvi, K., Pattabhi, S. & Kadirvelu, K. 2001 Removal of Cr(VI) from aqueous solution by adsorption onto activated carbon. *Bioresource Technology* **80** (1), 87–89. https://doi.org/10.1016/S0960-8524(01)00068-2.

Silveira, J. E., Barreto-Rodrigues, M., Cardoso, T. O., Pliego, G., Munoz, M., Zazo, J. A. & Casas, J. A. 2017 Nanoscale Fe/Ag particles activated persulfate: optimization using response surface methodology. *Water Science and Technology* **75** (9), 2216–2224. doi:10.2166/wst.2017.063.

Sohrabi, M. R., Amiri, S., Masoumi, H. R. F. & Moghri, M. 2014 Optimization of direct yellow 12 dye removal by nanoscale zero-valent iron using response surface methodology. *Journal of Industrial and Engineering Chemistry (Seoul, Korea)* **20** (4), 2535–2542. doi:10.1016/j.jiec.2013.10.037.

Su, Y., Adeleye, A. S., Keller, A. A., Huang, Y., Dai, C., Zhou, X. & Zhang, Y. 2015 Magnetic sulfide-modified nanoscale zerovalent iron (S-nZVI) for dissolved metal ion removal. *Water Research* **74**, 47–57.

Su, H., Fang, Z., Tsang, P. E., Zheng, L., Cheng, W., Fang, J. & Zhao, D. 2016 Remediation of hexavalent chromium contaminated soil by biochar-supported zero-valent iron nanoparticles. *Journal of Hazardous Materials* **318**, 533–540. doi:10.1016/j.jhazmat.2016.07.039.

Tang, Q., Wu, J., Lin, J., Li, Q. & Fan, S. 2008 Two-step synthesis of polyacrylamide/polyacrylate interpenetrating network hydrogels and its swelling/deswelling properties. *Journal of Materials Science* **43** (17), 5884–5890. doi:10.1007/s10853-008-2857-x.

Tsade, H., Anshebo, S. T., Sabir, F. K. & Singh, A. K. 2021 Preparation and characterization of functionalized cellulose nanomaterials (CNMs) for Pb(II) ions removal from wastewater. *Journal of Chemistry* **2021**, 5514853. doi:10.1155/2021/5514853.

Un, T., Kandemir, U., Erginel, A., & Ocal, N. & E, S. 2014 Continuous electrocoagulation of cheese whey wastewater: an application of response surface methodology. *Journal of Environmental Management* **146**, 245–250. doi:10.1016/j.jenvman.2014.08.006.

Wu, L., Liao, L., Lv, G. & Qin, F. 2015 Stability and pH-independence of nano-zero-valent iron intercalated montmorillonite and its application on Cr(VI) removal. *Journal of Contaminant Hydrology* **179**, 1–9. doi:10.1016/j.jconhyd.2015.05.001.

Xie, Y. & Cwiertny, D. M. 2010 Use of dithionite to extend the reactive lifetime of nanoscale zero-valent iron treatment systems. *Environmental Science & Technology* **44** (22), 8649–8655. doi:10.1021/es102451t.

Xu, J., Avellan, A., Li, H., Clark, E. A., Henkelman, G., Kaegi, R. & Lowry, G. V. 2020a Iron and sulfur precursors affect crystalline structure, speciation, and reactivity of sulfidized nanoscale zerovalent iron. *Environmental Science & Technology* **54** (20), 13294–13303. doi:10.1021/acs.est.0c03879.

Xu, J., Avellan, A., Li, H., Liu, X., Noel, V., Lou, Z., Wang, Y., Kaegi, R., Henkelman, G. & Lowry, G. V. 2020b Sulfur loading and speciation control the hydrophobicity, electron transfer, reactivity, and selectivity of sulfidized nanoscale zerovalent iron. *Advanced Materials* **32** (17). doi:10.1002/adma.201906910.

Yang, L., Gao, J., Liu, Y., Zhang, Z., Zou, M., Liao, Q. & Shang, J. 2018 Removal of methyl orange from water using sulfur-modified nZVI supported on biochar composite. *Water, Air, & Soil Pollution* **229** (11). doi:10.1007/s11270-018-3992-x.

Zhang, W. 2003 Nanoscale iron particles for environmental remediation: an overview. *Journal of Nanoparticle Research* **5** (3), 323–332. doi:10.1023/A:1025520116015.

Zhang, X., Lin, S., Chen, Z., Megharaj, M. & Naidu, R. 2011 Kaolinite-supported nanoscale zero-valent iron for removal of Pb^{2+} from aqueous solution: reactivity, characterization and mechanism. *Water Research* **45** (11), 3481–3488. doi:10.1016/j.watres.2011.04.010.

Zhang, Y., Tian, Z., Jing, Q., Chen, Y. & Huang, X. 2019 Removal of Cr(VI) by modified diatomite supported NZVI from aqueous solution: evaluating the effects of removal factors by RSM and understanding the effects of pH. *Water Science and Technology* **80** (2), 308–316. doi:10.2166/wst.2019.275.

Zheng, P., Wang, L., Chen, X., Wei, X., Liang, J. & Wu, J. 2020 Excess gibbs energies and isothermal vapor–liquid equilibrium for citral + linalool, citral + α-pinene, and linalool + α-pinene systems using headspace gas chromatography. *Journal of Chemical & Engineering Data* **65** (7), 3593–3604. doi:10.1021/acs.jced.0c00172.

Zhu, F., Li, L., Ma, S. & Shang, Z. 2016 Effect factors, kinetics and thermodynamics of remediation in the chromium contaminated soils by nanoscale zero valent Fe/Cu bimetallic particles. *Chemical Engineering Journal* **302**, 663–669. doi:10.1016/j.cej.2016.05.072.

Zhu, F., Li, L., Ren, W., Deng, X. & Liu, T. 2017 Effect of pH, temperature, humic acid and coexisting anions on reduction of Cr(VI) in the soil leachate by nZVI/Ni bimetal material. *Environmental Pollution* **227**, 444–450. doi:10.1016/j.envpol.2017.04.074.

First received 23 May 2021; accepted in revised form 20 July 2021. Available online 4 August 2021